Progress In Electromagnetics Research, Vol. 125, 483–501, 2012

A NOVEL NARROW BANDPASS FILTER FOR IMAGE REJECTION AND CHANNEL SELECTION IN A WIRELESS SLEEP APNOEA MONITORING SYSTEM

Y. Yang*, S. M. Roy, N. C. Karmakar, and X. Zhu

Department of Electrical and Computer Systems Engineering, Monash University, Building 72, Clayton Campus, Melbourne, VIC 3800, Australia

Abstract—A highly compact bandpass filter (BPF) is designed with a capacitively-coupled compact ring resonator. The ground plane is perturbed with a combination of two inter-digital and two spiral defected ground structures (DGSs), which enhance the selectivity and suppress the higher order harmonics of the BPF respectively. The filter has a selectivity of 0.22 dB/MHz, passband insertion loss (IL) of 1.55 dB and bandwidth of 61 MHz at 2.53 GHz. The proposed compact ring resonator yields a size reduction of 70.5% compared to a conventional ring resonator. This BPF is significant for wireless telemetry monitoring systems for physiological parameters including electrocardiogram (ECG), electroencephalography (EEG) and electromyography (EMG) using portable devices.

1. INTRODUCTION

Filter technology plays a significant role in the research field of modern communication devices. In response to the needs from various communication systems, microwave passive filters are widely developed and studied in [1–7]. However, these designs have not clearly presented their exact applications, especially the performances, in communication systems. In contrast to these designs, this paper introduces a compact passive bandpass filter (BPF) with high selectivity and high quality factor (Q factor) operating at radio frequency (RF) of 2.5 GHz for the wireless transmission of physiological parameters. This BPF is specially designed in a sleep apnoea monitoring system for channel selection and signal image rejection purpose.

Received 29 January 2012, Accepted 17 February 2012, Scheduled 7 March 2012

* Corresponding author: Yang Yang (yang.yang@monash.edu).

In this design, we also want to reduce the interference from other applications such as Wi-Fi (operating at 5.2 GHz) and UWB (operating from 3.1 GHz to 10 GHz), as the sleep apnoea monitoring process may be conducted in the patient's home where Wi-Fi or UWB local area network (LAN) might exist (for example, a home network organized by a wireless router). Moreover, the high order harmonics have to be suppressed so that the signal to noise ratio (SNR) can be maximized in the available industrial, scientific and medical (ISM) band for transmitting other physiological parameters. To meet these stringent physical and electrical requirements, we have developed a novel capacitively-coupled high-Q ring BPF with meta-materials in the form of inter-digital and spiral DGSs. The new design offers all required specifications such as compact size, high selectivity and suppression of higher order harmonics. Table 1 shows the design specification for this project.

Among different RF bandpass filter structures, microstrip circular and ring resonators are inherently high-Q devices. Microstrip ring resonators in particular have a wide range of applications in wireless communication [8, 9] due to their simple and flexible topologies (variants), ease of tuning and low profiles. Circular ring resonators also feature good transmission characteristics, high selectivity and flat passband response [10]. However, excitation of the resonator needs special treatment. Simple capacitive coupling with microstrip transmission lines results in poor coupling. Mao et al. [11, 12] proposed a V-shaped coupling arm and inter-digital coupling to address this problem. Many other coupling methods are discussed in [13]. We have introduced a novel coupling method for maximum coupling and two different varieties of DGSs to enhance selectivity and suppression of higher order harmonics. At the same time, we have saved a real estate of 138 mm^2 and obtained 0.22 dB/MHz selectivity and 61 MHz bandwidth at 2.45 GHz. The measured passband insertion loss is 1.55 dB and the in-band return loss is 16 dB. Therefore, the objective of a high performance compact circular BPF, which is compatible with our proposed wireless ECG transducer, has been fulfilled.

The paper is organized as follows: Section 2 introduces the objective of a compact, high-Q, high selectivity BPF with the

Table 1. Design specifications of the proposed BPF.

Radius size	Selectivity	Passband centre frequency	2nd harmonic suppression at	3rd harmonic suppression at
7.6 mm	0.22 dB/MHz	2.45 GHz	4.97 GHz	7.8 GHz

application background. Section 3 shows the design of the novel BPF. The simulated and measured results are discussed in Section 4, followed by conclusions in Section 5.

2. DESIGN CONSIDERATIONS OF WIRELESS SLEEP APNOEA MONITORING SYSTEM

The development of a RF-based wireless transducer for monitoring sleep apnoea (SA) patients has been investigated in a previous paper [14] and a novel solution [15] to this specially required high performance BPF is presented in this paper. For the purpose of diagnosis and symptom analysis, doctors measure more than

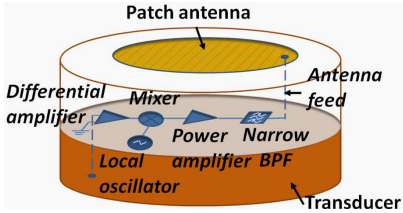

Figure 1. Proposed wireless transducer for physiological parameter measurement.

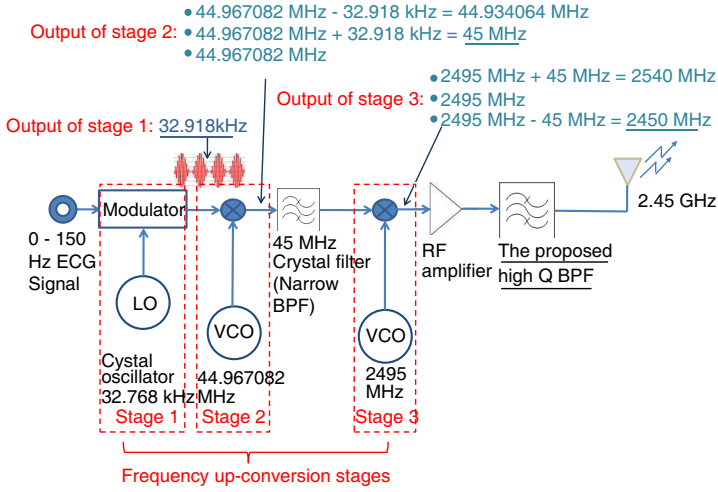

Figure 2. Block diagram of the proposed wireless ECG transducer.

eleven physiological parameters, such as electrocardiogram (ECG), electroencephalography (EEG) and electromyography (EMG), to diagnose a certain sleep-related disease. In our recently published work [16], the proposed wireless ECG transducer, as shown in Figure 1, is integrated with a differential amplifier, a frequency up-conversion circuit, a power amplification circuit, a high-selectivity BPF and a circular patch antenna. The base band ECG signal is up-converted to UHF (ultra high frequency) band with the processing of frequency modulation, up-conversion, amplification and filtering as shown in Figure 2. The proposed high-Q BPF filter plays a critical role in two stages: (a) image rejection/harmonic suppression in the frequency up-conversion stage as shown in Figures 2 and 3; (b) channel selection in the stage of RF communication. As shown in Figure 4, the proposed BPF can also be applied for channel selection in a 6-channel monitoring system for sleep apnoea diagnosis [14]. In this system, the 6 channels are allocated for different physiological parameters within a very narrow frequency band. As has been introduced in [14], this solution can reduce the power consumption and cost of the overall system.

In this project, we need a very compact circular filter that conforms to the geometrical shape of the circular transducer. We select a high-Q ring resonator as basic part of the BPF. According to our proposed transmission-link design in Figure 2, the ECG signal (less than 150 Hz) is frequency up-converted via three essential stages. The output of stage 3 contains three signals: the expected 2.45 GHz signal, the undesired 2.54 GHz image signal and the 2.495 GHz local

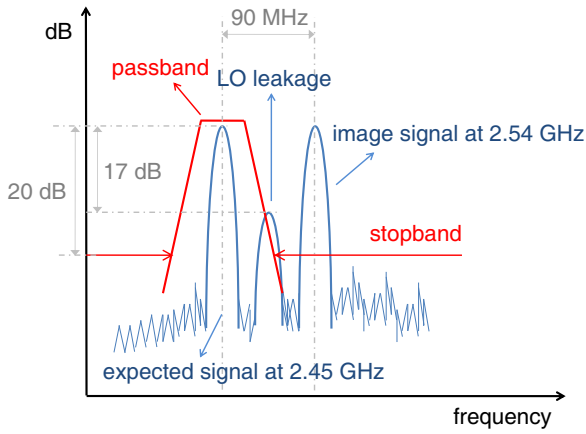

Figure 3. Required performance of the proposed BPF.

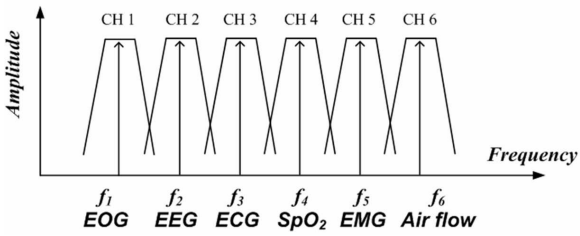

Figure 4. Channel allocation for sleep apnoea diagnosis.

oscillator (LO) leakage signal. In this project, the mixer used in stage 3 is an ADE-30 W produced by Mini-Circuits^{TM}. According to the datasheet of the ADE-30W, the minimum LO-RF isolation is 17 dB, which means the LO leakage is attenuated at least 17 dB at the RF output port. Therefore, the 2.54 GHz image signal becomes the main interference rather than the LO leakage. Figure 3 shows the required filter performance on the RF output. In order to effectively eliminate the impact of the image signal, it is necessary to attenuate the image signal (2.54 GHz) at least 20 dB from the expected RF signal (2.45 GHz). This requires the proposed BPF to satisfy a selectivity of 0.22 dB/MHz (derived from 20 dB divided by 90 MHz). The required high selectivity has been successfully achieved by using inter-digital defected ground structure (DGS) and its performance is presented in the results section.

3. DESIGN OF DGS ENGINEERED RING RESONATOR BPF

3.1. Design of Compact Ring Resonator

The design procedure of a ring resonator has been comprehensively investigated in [13, 17, 18]. A conventional ring resonator excited by two gap-coupled microstrip lines suffers from poor capacitive coupling. Figure 5(a) shows a conventional ring resonator with two capacitively-coupled microstrip lines. The coupling between the feed-line and the ring resonator is proportional to the length of coupling area and the coupling gap width. Therefore, efficient coupling with low insertion loss becomes difficult to achieve in this conventional coupling method. To improve the coupling, we have indented the ring resonator and inserted the feed-line inside the indentation. The outcome is two-fold — the most efficient coupling and compact design. Both are most desirable features for our designed wireless ECG transducer. Figure 5(b) shows

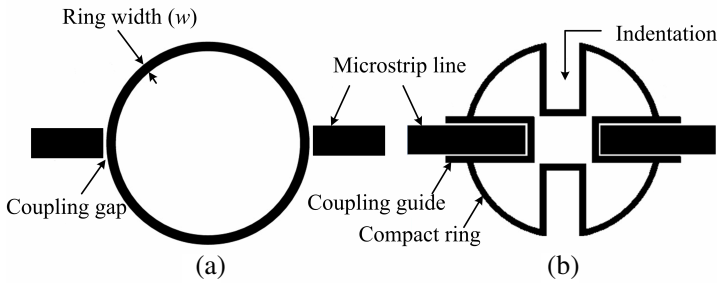

Figure 5. Layout of (a) a conventional circular ring resonator and (b) a proposed compact ring resonator with coupling guides and insertion slots.

Table 2. Dimensional comparison between conventional and compact ring resonators designed at 2.45 GHz.

Type of resonator	Ring radius (mm)	Microstrip line width (mm)	Track width of ring (mm)	Coupling gap width (mm)
Conventional ring	$R_1 = 14$	2.25	0.5	0.2
Compact ring	$R_2 = 7.6$	2.25	0.5	0.2

Table 3. Dimensions of the spiral DGSs (in millimeters).

a	**b**	**c**	**d**	**e**	**f**	**g**
0.9	0.4	1	0.5	0.7	3	0.3

the proposed indented and capacitively-coupled ring resonator.

The design was optimized by using Agilent full wave EM solver ADS Momentum^{TM}. An excellent coupling between the feed-line and the ring resonator has been achieved, and the results are presented in Section 4. Table 2 shows the dimensional comparison of the conventional and compact ring resonators designed at 2.45 GHz. The percentage of saved area is calculated by:

$$A = \frac{\pi \times R_1^2 - \pi \times R_2^2}{\pi \times R_1^2} = 70.53\% \tag{1}$$

where π is circumference-to-diameter ratio, R_1 and R_2 are the radii of the conventional and compact ring resonators respectively and A is the percentage of saved area. It shows that the overall dimension of the compact ring resonator has been reduced by approximately 70.5%

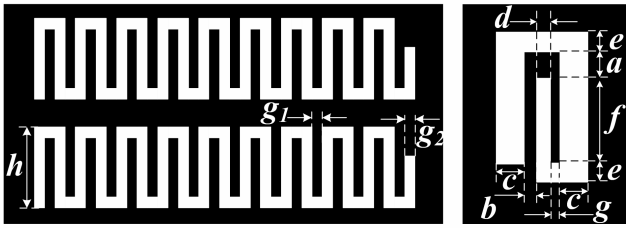

Figure 6. Layout and dimensional parameters of (a) two inter-digital DGSs and (b) a spiral DGS.

compared to the conventional resonator. The radius of the conventional ring resonator is calculated from (1) and the track width is optimized from Table 4.

3.2. Inter-digital and Spiral DGSs

After obtaining optimum coupling between the ring resonator and the feed-lines, two types of DGS are needed to improve the selectivity and suppress the higher order harmonics. Conventional dumbbell-shaped DGSs are lowpass Butterworth filters [19]. However, they suffer from narrow stopband characteristics and are not suitable to suppress multiple higher order harmonics for a BPF [19]. In this design, we propose two advanced DGSs in the form of spiral and inter-digital perturbations on the ground plane. The spiral loaded bandstop filters have been comprehensively studied for our chipless RFIDs in [20–24]. Figure 6(a) shows two inter-digital DGS slots on a ground plane. The gap between the inter-digital fingers offers the capacitance. The extra inductance is generated by the inter-digital fingers due to the perturbed and elongated current paths. As introduced in [25], two or more inter-digital DGS slots can generate a lowpass characteristic with a relatively high selectivity, while the selectivity is tunable within a certain range by changing the width of the inter-digital slots and fingers.

The proposed dimensions for the inter-digital DGS structure are shown in Figure 6(a), where g_1 is the width of the slots of the inter-digital DGS and g_2 is the width of the metal fingers between the slots. For easier fabrication, both the values of g_1 and g_2 are set to 0.3 mm. The depth of the stopband is directly affected by the height of the interdigital DGS. To achieve deep band-rejection characteristics, the height h is tuned to 3.75 mm. The band-rejection range is tuned by increasing/reducing the number of finger slots. To generate a narrow

passband with relatively high selectivity, the inter-digital structure is applied under one side of the microstrip line, avoiding coupling with the compact ring (a 3-D view is given in Figure 7). Figure 6(b) shows the layout of the proposed spiral DGS. The slot gaps control the gap capacitance between the current element, while the width and length of the metal-strips control the effective inductance of the spiral DGS.

3.3. Integrated DGS Engineered Ring Resonator Filter

Once both DGSs had been designed to their optimum performances (as shown in Section 4), the DGSs were integrated into the ground plane of the proposed compact ring resonator. Figures 7(a) and (b) show the inter-digital only, and inter-digital and spiral DGS engineered compact ring filters, respectively. In each stage, Agilent ADS Momentum was used to optimize the design to meet the performance requirements.

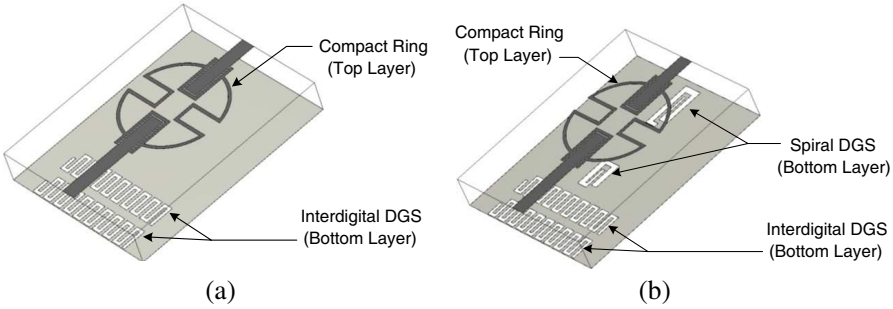

Figure 7. Isometric views of (a) inter-digital and (b) inter-digital and spiral DGS engineered compact ring BPF.

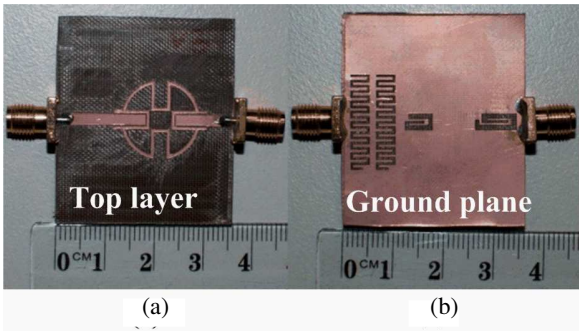

Figure 8. Fabricated compact BPF with inter-digital and spiral DGSs: (a) top view and (b) bottom view.

Table 3 shows the design parameters of the spiral DGS. Figure 8 shows photographs of the final prototype of the BPF.

4. RESULTS AND DISCUSSION

After the design of the two DGS engineered BPFs was optimized, the BPF was fabricated on commercial microwave substrate TLX-0 and tested using Agilent performance network analyzer (PNA) E8361A with full two-port error correction calibration and confidence check. This section presents the simulated and measured results of the design procedure, and discussions of: (i) a compact ring resonator; (ii) selectivity enhancement by using inter-digital DGS; (iii) harmonics suppression by using spiral DGS and (iv) performance investigation of the proposed BPF by integrating these components.

4.1. Ring Resonator

The objectives of this compact ring design are: (i) improving coupling to reduce insertion loss; and (ii) compacting the dimensions by indentation in four orthogonal positions with respect to the capacitively-coupled inset feed-lines. The design process started by analyzing a conventional ring resonator shown in Figure 5(a), and then a conventional ring resonator was modified into a compact ring resonator, as shown in Figure 5(b).

To analyze the conventional ring resonator, comprehensive investigation was carried out to optimize coupling (transmission)

Table 4. Performance variation of the conventional circular ring resonator for different (w/h) ratio and radii.

Radius of the ring resonator (mm)	Track width (w) of the ring resonator (mm)	(w/h) ratio	Simulation results (ADS Momentum)		
			Resonant freq. (GHz)	Insertion loss S_{21} (dB)	3-dB bandwidth (MHz)
13.9	1	> 1	2.421	-10.61	14
13.8	1.5	> 1	2.418	-11.551	14
13.7	2	> 1	2.421	-12.549	14
14.26	0.3	< 1	2.426	-12.495	22
14.21	0.4	< 1	2.422	-11.521	19.5
14.16	0.5	< 1	2.42	-11.11	19

Substrate: Taconic TLX-0 ($\varepsilon_r = 2.45$, $\tan\delta = 0.0019$, thickness $= 0.787$ mm); coupling gap: 0.2 mm

performance. In this investigation, the designed centre-frequency of the circular ring resonator was 2.45 GHz. For clarity, Table 4 shows the variation of the simulated insertion loss of the circular ring resonator shown in Figure 5(a) for different w/h ratios. It is observed that the comparatively narrowband properties are exhibited for $w/h > 1$. The track width of the ring does not significantly influence the magnitude of the insertion loss (S_{21}) parameter, but it has slight influence on the resonant frequency. This property can be used for fine adjustment of the ring resonator. The great advantage of our design compared to that in [12] is that we are not perturbing the heart of the filter — the compact ring resonator — to suppress the higher order harmonics. The frequency shift is therefore minimized in our design. As a consequence the redesign of a filter for large frequency shift compensation as reported in [12] is not required in our work.

Table 4 shows that the insertion loss was observed to be greater than 10 dB for all investigated cases with a coupling gap of 0.2 mm (conventional coupling). As slot width less than 0.2 mm was difficult to realize with conventional microwave laminates, 0.2 mm was used as the coupling gap in this design. After a series of investigations of the depth of the indentation and length of the coupling guide, we found that the insertion loss of the fundamental passband could be reduced to less than 0.9 dB by setting the length of the indentation plus coupling guide length to 7.83 mm.

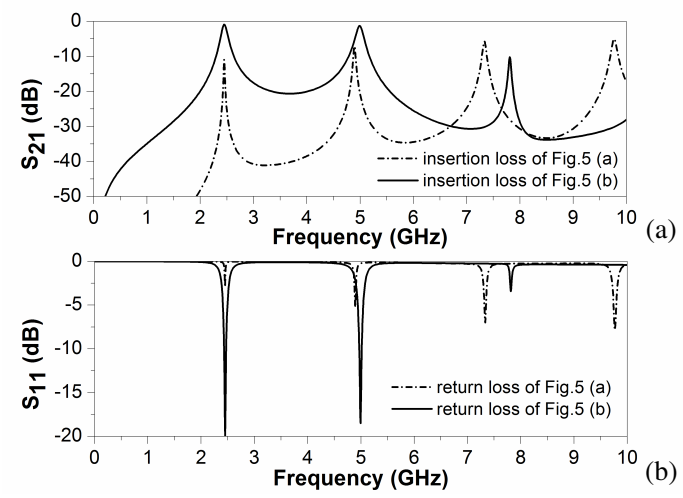

Figure 9. Simulated frequency responses of conventional and proposed compact ring resonators: (a) S_{21} and (b) S_{11}.

Table 2 shows the design parameters of the structures shown in Figures 5(a) and (b), respectively. Based on these parameters, the comparison of the simulation of the frequency responses between the conventional and our proposed ring resonators was investigated.

Figure 9 shows the return loss and insertion loss vs frequency plots based on the ring resonators in Figure 5. The passband transmission (S_{21}) or coupling coefficient at resonances is significantly improved from merely 11 dB for the case of a conventional circular ring resonator (shown in Figure 5(a)) to 0.9 dB for the proposed compact ring resonator (shown in Figure 5(b)). Significant improvement has also been observed in the return loss plot (from merely 2.5 dB to more than 20 dB at the fundamental frequency of 2.45 GHz). This clearly indicates that the proposed compact ring resonator can provide a strong coupling effect compared to the conventional ring resonator. Having investigated the improved performance by the proposed compact ring resonator, next we move to the analysis of the DGSs performance.

4.2. Inter-digital DGS and Improved Selectivity of BPF

It has been found from our study that a single inter-digital DGS can generate a single transmission zero with slow roll-off, while three inter-digital DGS may cause problem for harmonics suppression in stopband. In contrast, two inter-digital DGS can achieve the best selectivity without deteriorating the BPF performance.

According to another study on the effect of the inter-digital DGS on the BPF performance, a varying distance between the two adjacent DGS slots can lead to a frequency-shift of the transmission zeros generated by the DGS slots. In this design, the distance between the two inter-digital DGS is optimized and tuned to 1.25 mm for acquiring the best selectivity and harmonic-suppression.

As shown in Figure 9, the fundamental passband generated by the compact ring resonator gives a selectivity of 22.5 dB/GHz. This is not acceptable for our proposed up-conversion transmission link (refer to Figure 2) due to the fact that the difference between the designed frequency 2.45 GHz and its image frequency 2.54 GHz is 90 MHz which is too narrow for the compact ring BPF to filter out the undesired image frequency (as shown in Figure 3). Figure 10 shows the comparison of the simulated results of the compact ring BPF with and without inter-digital DGSs. It is clear that, by incorporating two inter-digital DGS slots in the ground plane, the selectivity of the BPF has been significantly increased by 10 times compared to the BPF without inter-digital DGS slots. The measured selectivity is very close to the simulated value of 0.22 dB/MHz. Thus, the specified requirements of

the transmission-link design as shown in Figures 2 and 3 have been achieved.

4.3. Spiral DGS

The effect of the two spiral DGS on the BPF performance versus the distance between them has been comprehensively studied. According to our study, the distance between the two spiral DGS may lead to a frequency-shift of transmission zeros generated by the spiral DGS. This may lead to difficulty in fully suppressing the 2nd and 3rd harmonics. To obtain the best harmonic-suppression effect, the distance between the two spiral DGS has been fixed to 8.4 mm through fine-tuning.

As mentioned above, the higher order harmonics (2nd and 3rd) can be eliminated by placing the spiral DGS slots under the microstrip feed-lines. The spiral DGS has the advantage of compact size and is easy to tune for a wide range of frequencies. Based on the simulated results in Figure 9, the 2nd and 3rd order harmonics are generated at 4.97 GHz and 7.8 GHz, respectively. These two harmonics can be removed by the proposed spiral DGS shown in Figure 6(b). The dimensions of the spiral DGS are listed in Table 3. By increasing the total length of the spiral slot, the resonant frequency of 4.97 GHz can be easily achieved. The widths of the spirals do not exceed the width of the microstrip line. Therefore, the capacitive coupling between the microstrip line and compact ring is not affected by the spiral DGS slots. Figure 7(b) shows the placement of the spiral DGS slots in the ground plane of the proposed BPF. Consistent with the simulated results in Figure 11, the

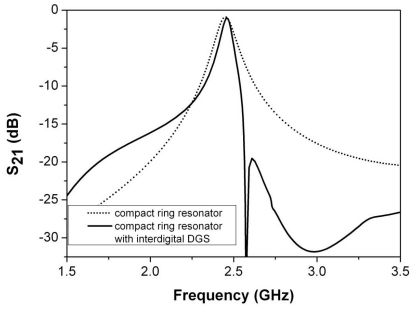

Figure 10. Simulated frequency responses (S_{21}) of proposed compact ring resonator with (solid line) and without (dotted line) inter-digital DGS.

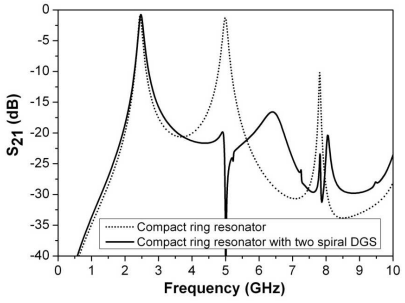

Figure 11. Simulated frequency responses (S_{21}) of a compact ring resonator with (solid line) and without (dotted line) the designed spiral DGSs.

2nd and 3rd order harmonics are successfully eliminated by placing the designed two spiral DGS slots.

4.4. Inter-digital and Spiral DGSs Engineered BPF

After obtaining satisfactory performance from the separate integrations of the two DGS types as shown in Figures 10 and 11, both DGSs were integrated with the BPF. The performance was optimized using ADS and the results are presented in Figure 12. It can be observed from Figure 12 that the simulated insertion loss is 1.2 dB at 2.45 GHz and the measured insertion loss is 1.55 dB at 2.53 GHz with a 3-dB passband bandwidth of 61.1 MHz. This minor frequency shift was due to the fabrication tolerance and simulation precision which was also encountered by two other research groups [12, 19]. Both the simulated and measured selectivities were calculated as 0.22 dB/MHz. This successfully achieves the design specification in Table 1 for the proposed wireless ECG telemetry transmission link. There may be some radiation leakage in the frequency range from 4.6 GHz to 6.4 GHz due to high return loss in the order of average 8 dB. However, this problem

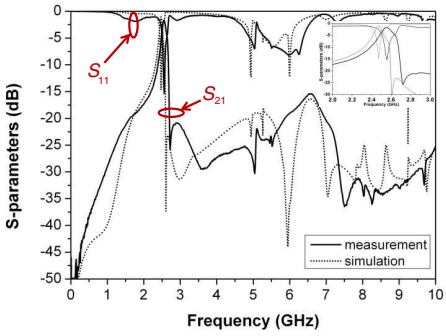

Figure 12. Comparison of the frequency response between simulation and measurement of the proposed BPF.

Table 5. Comparison of the measured filter performance among different designs using microstrip ring resonator.

Filter performance	Ma [10]	Mao [11]	Mao [12]	This work
Passband insertion loss (dB)	2	3.6	2.49	1.55
Passband return loss (dB)	10	12	17	16
Selectivity (dB/MHz)	≤ 0.071	0.096	0.25	0.22
Group delay in passband (ns)	-	-	-	2.9

can be improved by adding extra DGS with stopband at that frequency range, as described in [26]. Table 5 shows our superior coupling performance compared with other work [10–12]. The next investigation is on the non-linear phase response of the filter due to incorporation of the spiral and inter-digital DGSs.

4.5. Group Delay Investigation

Since the goal of the design is to obtain high selectivity at the upper cutoff frequency, high group delay at the transmission zero may create

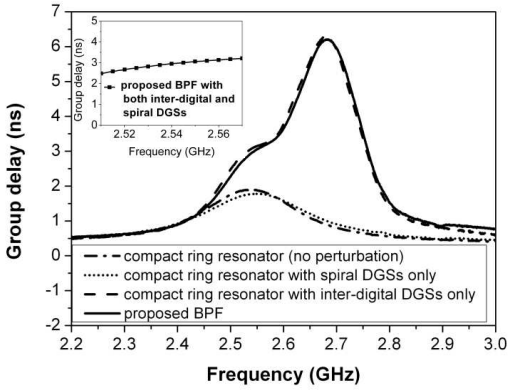

Figure 13. Measured results of group delay in four different conditions.

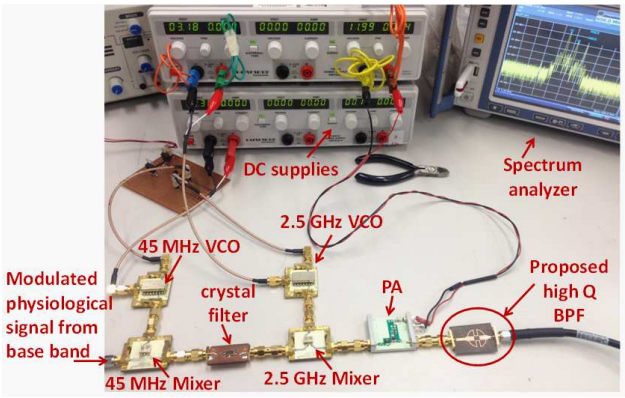

Figure 14. Testing of a proposed BPF in a 2.5 GHz RF transducer prototype.

high phase non-linearity. Therefore, a comprehensive experimental investigation into the group delay of the designed filter was conducted. The group delay of the filter was measured under four different conditions: (a) the compact ring resonator, (b) the compact ring resonator with spiral DGSs only, (c) the compact ring resonator with the inter-digital DGSs only and finally (d) the proposed BPF — the compact ring resonator with both spiral and inter-digital DGSs. The group delays were measured on Agilent PNA and the measured results are presented in Figure 13. As can be seen in Figure 13, the values of group delay are 1.88 ns and 1.75 ns for the cases of (a) no perturbation and (b) with spiral DGSs at the center frequency of the passband

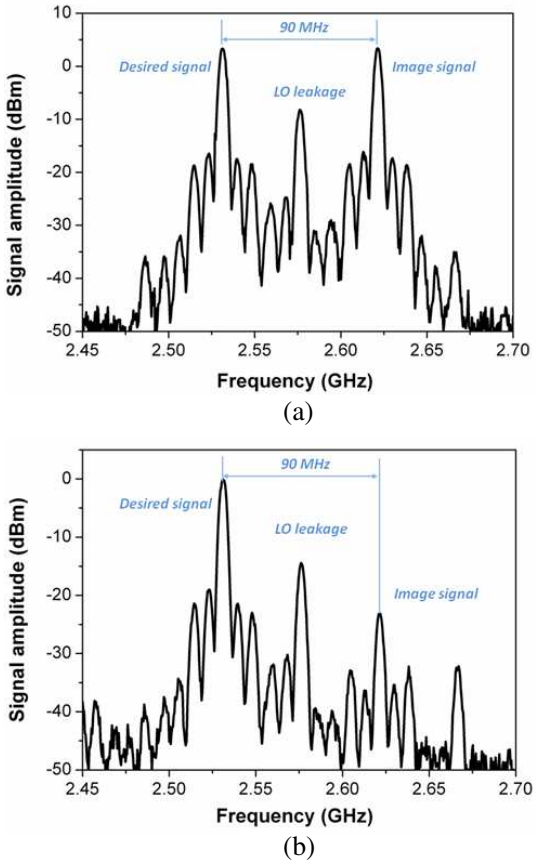

Figure 15. Measured output of the 2.5 GHz baseband-to-RF transducer prototype: (a) without proposed BPF and (b) with a proposed BPF.

(2.54 GHz). However, with (c) the inter-digital DGSs, the group delay increases to 3.08 ns at 2.54 GHz and continuously rises to 6.2 ns at the 2.69 GHz (location of transmission zero). This clearly proves that the inter-digital DGSs are predominant for high selectivity behavior of the filter at the expense of large group delay. Similar results are also reported in [27].

As is shown in the inset of Figure 13, a relatively flat group delay was achieved in the passband from 2.51 GHz to 2.57 GHz. This clearly shows that this design has successfully achieved the specified high selectivity with a reasonably acceptable linear-phase response within the passband. This has significance for compact microstrip filter design for high selectivity purposes.

4.6. Bandpass Filter Performance

As is shown in Figure 14, the performance of the proposed BPF was tested in a proposed baseband-to-RF transducer prototype which has been explained in the block diagram in Figure 2. The measured filter performance has been presented in Figure 15. According to Figure 15, the image signal was significantly attenuated by 24 dB. Therefore, this design successfully realized the requirements specified in Figure 3.

5. CONCLUSION

New and emerging technological developments present challenging specification requirements. Our ARC Linkage Project on wireless sleep apnoea monitoring is one project where a very compact but high selectivity and high order harmonic suppressing BPF is an essential component for the integrity of channel selection for various physiological parameters. This unique requirement has forced us — the RF and microwave design engineers — to design a novel BPF in a compact package.

To achieve the stringent design goal in a small package, we have taken novel approaches to passive circuit designs based on modern microwave technologies. The new findings are: (i) the generic ring resonator filter has been pushed for the maximum coupling (for minimum passband insertion loss) by indenting the ring into four orthogonal places and inserting the feed-lines into the indentations. This modification not only improves the coupling with the feed-lines but also reduces the design dimension by 70.5%. (ii) Only < 2 dB measured passband insertion loss is obtained in such a compact passive BPF. It is a remarkable achievement to improve the efficacy of the wireless transmission system by reducing the dependency on a power

amplifier to compensate for the passive filter loss. (iii) Thirdly, the other unique filter performance requirements of (a) high selectivity for image frequency rejection and (b) high order harmonics suppression for channel integrity between various physiological parameters have been achieved with two newly-designed DGSs (inter-digital and spiral) on the ground plane of the BPF. It is interesting to observe from the group delay measurement of the designed filter that the filter enjoys reasonably acceptable group delay of around 2 ns within the passband. (iv) Finally, minimum frequency retuning is required in our approach because we are not perturbing the compact ring resonator structure, in contrast to [12]. This novel approach to the compact high selectivity passive filter not only advances the knowledge base of implementing novel DGSs in various microwave passive designs [26] but also builds confidence in the development of new challenging technologies.

ACKNOWLEDGMENT

The authors wish to acknowledge the assistance and support of Regni Pty. Ltd. Special thanks to Uditha Bandara for his technical support during the design process.

REFERENCES

1. Wei, C. L., B.-F. Jia, Z.-J. Zhu, and M. Tang, "Design of different selectivity dual-mode filters with E-shaped resonator," *Progress In Electromagnetics Research*, Vol. 116, 517–532, 2011.
2. Ho, M.-H. and P.-F. Chen, "Suspended substrate stripline bandpass filters with source-load coupling structure using lumped and full-wave mixed approach," *Progress In Electromagnetics Research*, Vol. 122, 519–535, 2012.
3. Xu, Z., J. Guo, C. Qian, and W.-B. Dou, "A novel quasi-elliptic waveguide transmit reject filter for Ku-band VSAT transceivers," *Progress In Electromagnetics Research*, Vol. 117, 393–407, 2011.
4. Guodos, S. K., Z. D. Zaharis, and T. V. Yioultsis, "Application of a differential evolution algorithm with strategy adaptation to the design of multi-band microwave filters for wireless communications," *Progress In Electromagnetics Research*, Vol. 109, 123–137, 2010.
5. Cui, D., Y. Liu, Y. Wu, S. Li, and C. Yu, "A compact bandstop filter based on two meandered parallel-coupled lines," *Progress In Electromagnetics Research*, Vol. 121, 271–279, 2011.

6. Zhang, Q.-L., W.-Y. Yin, S. He, and L.-S. Wu, "Evanescent-mode substrate integrated waveguide (SIW) filters implemented with complementary split ring resonators," *Progress In Electromagnetics Research*, Vol. 111, 419–432, 2011.
7. Wu, Y., Y. Liu, S. Li, and C. Yu, "A new wide-stopband low-pass filter with generalized coupled-line circuit and analytical theory," *Progress In Electromagnetics Research*, Vol. 116, 553–567, 2011.
8. Ramirez, R. R. and N. G. Alexopoulos, "Single feed circularly polarised microstrip ring antenna and arrays," *IEEE Antennas and Propagation Society International Symposium*, Vol. 3. 1364–1367, 1998.
9. Gil, I., J. Garcia-Garcia, J. Bonache, F. Martin, M. Sorolla, and R. Marques, "Varactor-loaded split ring resonators for tunable notch filters at microwave frequencies," *Electronics Letters*, Vol. 40, No. 21, 1347–1348, 2004.
10. Ma, Z., C.-P. Chen, and T. Anada, "Microwave and millimeter-wave UWB banpass filters using microstrip ring resonators," *2010 International Symposium on Signals Systems and Electronics, ISSSE*, 1–4, 2010.
11. Mao, R.-J. and X.-H. Tang, "Novel dual-mode bandpass filters using hexagonal loop resonators," *IEEE Transactions on Microwave Theory and Techniques*, Vol. 54, No. 9, 3526–3533, 2006.
12. Mao, R.-J., X.-H. Tang, and F. Xiao, "Miniaturized dual-mode ring bandpass filters with patterned ground plane," *IEEE Transactions on Microwave Theory and Techniques*, Vol. 55, No. 7, 1539–1547, 2007.
13. Chang, K., *Microwave Ring Circuits and Antennas*, John Wiley & Sons, Inc., 1996.
14. Yang, Y., N. C. Karmakar, and X. Zhu, "A portable wireless monitoring system for sleep apnoea diagnosis based on active RFID technology," *Proc. IEEE Asia Pacific Microwave Conference*, Melbourne, Dec. 6, 2011.
15. Yang, Y., S. M. Roy, N. C. Karmakar, and X. Zhu, "A novel high selectivity bandpass filter for wireless monitoring of sleep apnoea patients," *Proc. IEEE Asia Pacific Microwave Conference*, Melbourne, Dec. 8, 2011.
16. Karmakar, N. C., Y. Yang, and I. T. Brown, "Wireless passive radio frequency based monitoring system for sleep apnoea patient (especially paediatric patients)," *Engineering and Physical Sciences in Medicine and the Australian Biomedical Engineering Conference*, 51–52, 2009.

17. Getsinger, W. J., "Microstrip dispersion model," *IEEE Transactions on Microwave Theory and Techniques*, Vol. 21, No. 1, 34–39, 1973.
18. Kirschning, M. and R. H. Jansen, "Accurate model for effective dielectric constant of microstrip with validity up to millimetre-wave frequencies," *Electronics Letters*, Vol. 18, No. 6, 272–273, 1982.
19. Ahn, D., J. S. Park, C. S. Kim, J. Kim, Y. Qian, and T. Itoh, "A design of the low-pass filter using the novel microstrip defected ground structure," *IEEE Transactions on Microwave Theory and Techniques*, Vol. 49, No. 1, 86–93, 2001.
20. Preradovic, S., I. Balbin, N. C. Karmakar, and G. F. Swiegers, "Multiresonator-based chipless RFID system for low-cost item tracking," *IEEE Transactions on Microwave Theory and Techniques*, Vol. 57, No. 5, 1411–1419, 2009.
21. Preradovic, S. and N. C. Karmakar, "Design of chipless RFID tag for operation on flexible laminates," *IEEE Antennas and Wireless Propagation Letters*, Vol. 9, 207–210, 2010.
22. Preradovic, S., S. Roy, and N. C. Karmakar, "Fully printable multi-bit chipless RFID transponder on flexible laminate," *Asia Pacific Microwave Conference*, 2371–2374, 2009.
23. Roy, S., "Development of a frequency encoded chipless RFID tag," Ph.D. Thesis, Dept. of Electrical and Computer Systems Engineering, Monash University, 2008.
24. Karmakar, N. C., S. M. Roy, and I. Balbin, "Quasi-static modeling of defected ground structure," *IEEE Transactions on Microwave Theory and Techniques*, Vol. 54, No. 5, 2160–2168, 2006.
25. Balalem, A., A. R. Ali, J. Machac, and A. Omar, "Quasi-elliptic microstrip low-pass filters using an interdigital DGS slot," *IEEE Microwave and Wireless Components Letters*, Vol. 17, No. 8, 586–588, 2007.
26. Karmakar, N. C. and M. N. Mollah, "Investigations into nonuniform photonic-bandgap microstripline low-pass filters," *IEEE Transactions on Microwave Theory and Techniques*, Vol. 51, No. 2, 564–572, 2003.
27. Hao, Z.-C., J.-S. Hong, J. P. Parry, and D. P. Hand, "Ultra wideband bandpass filter with multiple notch bands using nonuniform periodical slotted ground structure," *IEEE Transactions on Microwave Theory and Techniques*, Vol. 57, No. 12, 3080–3088, 2009.